Ultra-highly sensitive DNA detection with conducting polymer-modified electrodes: mechanism, manufacture and prospects for rapid e-PCR

Bicheng Zhu[a,b], Thomas Kerr-Philips[a], Zahraa Al Ghaus[a], Eddie Wai Chi Chan[a,b], David Barker[a,b], Clive W. Evans[a,c], David E. Williams,[* a,b] Jadranka Travas-Sejdic[*,a,b]

[a.] Polymer Biointerface Centre, School of Chemical Sciences, The University of Auckland, 23 Symonds Street, Auckland 1010, New Zealand
[b.] MacDiarmid Institute for Advanced Materials and Nanotechnology, Victoria University of Wellington, Laby Building Kelburn Campus Victoria University of Wellington, Wellington 6012, New Zealand
[c.] School of Biological Sciences, The University of Auckland, 24 Symonds Street, Auckland 1010, New Zealand

Email: david.williams@auckland.ac.nz and j.travas-sejdic@auckland.ac.nz

Abstract:

At low copy number, sequence detection by polymerase chain reaction (PCR) requires up to 30 cycles (amplification 10^9) to produce a reliably detectable concentration of fluorescently-labelled amplicons. The cycle number and hence detection time is determined by the analytical sensitivity of the detector. Hybridisation of complementary DNA strands to oligonucleotide-modified conducting polymer electrodes yields an increase in the charge transfer resistance for the ferri-ferrocyanide redox couple. We demonstrate sensors using screen-printed carbon electrodes modified with a conducting polymer formed from a monomer pre-functionalised with complementary oligonucleotide, with pM sensitivity for short sequences and aM for bacterial lysate, with a response time-scale of 5 min. The response is due to the variation of electrical resistance within the polymer film. We develop a mechanism based on repulsion from the solution interface of dopant anions by the charge associated with surface-bound DNA. With results for >160 single-use sensors, we formulate a response model based on percolation within a random resistor network and highlight challenges for large-scale manufacture of such sensors. Such sensors used for label-free electrochemical detection for PCR (e-PCR) would decrease the required cycle number from 30 to less than 10 and would offer a much simplified instrument construction.

Key words: polymerase chain reaction, PCR, conducting polymer, screen printed carbon electrode, DNA detection, percolation conductivity, sensor manufacture

1. Introduction

There is an urgent need to simplify and speed up DNA detection in clinical and environmental samples: the combination of polymerase chain reaction (PCR) with an electrochemical detection method is an attractive option for doing this since it offers a combination of a robust and specific amplification method with a simplified and sensitive detection instrument. Electrochemical methods for DNA sensing are indeed of great general interest, because of the simplicity, sensitivity and low cost of the measurement. Similarly, conducting polymers have been widely investigated as both sensing signal transducing substrates and as an anchor for biomolecular probes[1-5], for the optical or electrochemical detection of oligonucleotides (ONs)[6-11], proteins[12-14] and small molecular targets of biological interest, such as hormones[15, 16]. In terms of miniaturization and fabrication of portable sensing devices, electrochemical impedance spectroscopy (EIS) is often employed as a readout methodology, as it can detect minor changes in the properties of the electrode surface, including those induced by

biorecognition events. EIS has been widely used for the detection of biomolecules[1], including DNA[6, 8, 9], proteins[17] and whole cells[18]. Specifically, for DNA measurement, gold electrodes modified with self-assembled monolayers of thiolated oligonucleotides have been extensively studied[19-22]. Issues of stability of such electrodes have been well-documented[23]. The use of CPs with oligonucleotide covalently bound avoids at least some of these issues and in conjunction with EIS can detect ON hybridization with high sensitivity[4, 24]. The signal can be manipulated by altering the length[25], charge[26] and surface packing density of the capture probe[27]. Different mechanisms appear to operate over different concentration ranges: Donnan exclusion of the redox couple from the nanoporous interface[7] (the same mechanism as proposed for thiolated oligonucleotide-modified gold electrodes[19, 28]) and modulation of charge trapping in the polymer at the polymer-solution interface[7, 29], demonstrated by exploiting a nanowire in a configuration analogous to a liquid-gated field effect transistor. We developed this work into an electrochemical PCR method (e-PCR) that exploited the high sensitivity offered to yield results significantly faster than could be obtained with conventional fluorescence detectors[30]. More recently, we have developed a procedure for pre-attachment of ON probes onto CP monomers, thus opening the possibility of large-scale production of probe-functionalised sensors by simply applying a short potential pulse onto the electrode immersed in the monomer-ON solution. We demonstrated sensitive detection of short Non-Hodgkin lymphoma- and chronic lymphocytic leukemia-specific DNA sequences using either research-grade glassy carbon electrodes, gold electrodes or electrospun conductive mesh electrodes that had been surface-modified in this way[6, 8]

Sensitive and specific detection of bacterial contamination in food and water is a compelling target for sensor development. Farabullini et al. reported a disposable electrochemical gene sensor for the simultaneous analysis of different food-contaminating pathogenic bacteria by using thiol-labelled oligonucleotide probes immobilised on a screen-printed array with four gold electrodes[31]. Their sensor showed a negligible sensing response to *E. coli* genomic DNA by utilizing a *Salmonella* 12-mer oligonucleotide probe. Liao et al. reported an electrochemical sensor assay involving hybridization of DNA in *E. coli* bacterial lysates to both fluorescein-modified detector probes and biotin-modified capture probes anchored to a sensor surface. The length of capture probe in the electrode surface was a 35-mer[32]. The challenge, however, is the development of practical single-use, batch-calibrated devices of the required sensitivity and specificity that are mass-manufacturable. The development of portable and disposable biosensors and chemical sensors has largely utilised screen-printed electrodes (SPEs)[33-37]. Among SPEs, screen-printed carbon electrodes (SPCEs) are the most commonly used as they are inexpensive, suitable for industrial-scale manufacturing and have a wide potential window for electrochemical measurements [38]. There is a clear incentive to extend the studies of DNA measurement with conducting polymer-modified electrodes to SPEs, exploiting the idea of using pre-attachment of ON probes onto CP monomers, in order to explore the possible translation of this sensing technology, based on readily-fabricated, disposable sensing strips, into a commercial, portable and cost-effective device, particularly in its application as a detector for amplicons in PCR. However, there is a gap to fill in the understanding of the mechanism of response, particularly relating to the high sensitivity in conjunction with a wide dynamic range. The present work addresses that gap in understanding. Measurement of the response of a large number of disposable, CP-modified SPCEs and modelling the behavior as that of a random resistor network highlights challenges in repeatability of manufacture. We use a quartz-crystal microbalance to provide independent confirmation that DNA does indeed hybridise to the surface-conjugated probe.

2. Experimental

2. 1 Materials

Dimethylformamide (DMF), tetrahydrofuran (THF), phosphate buffered saline (PBS) pellets, sodium para toluene sulfonate (NaToS), potassium ferricyanide ($K_3[Fe(CN)_6]$), potassium ferrocyanide ($K_4[Fe(CN)_6]$), N-hydroxysuccinimide (NHS), and 1-ethyl-3-(3-dimethylaminopropyl) carbodiimide (EDC) were purchased from Sigma Aldrich. The carbon ink for screen-printed electrodes, BQ242, was purchased from DuPont. Kapton tape (No. 436-2778) and Mylar sheets (250 µm, No. 785-0802) were purchased from RS Components. Oligonucleotides (Table 1) were purchased from Alpha DNA. Phosphate-buffered saline solution (PBS) was prepared by dissolving a PBS tablet (P4417-100TAB, Sigma—Aldrich Ltd.) into 200 mL deionised water (Milli Q, 18.2 MΩ.cm at 25°C). Half-strength PBS (HPB) was made by mixing 200 mL PBS with 200 mL deionised water. Synthesis of (6,6′-((2,5-di(1H-pyrrol-2-yl)-1,4-phenylene)bisoxy)) dihexanoic acid (PyPhCOOH) and 2,2′-(2,5-bis(2-(2-(2-methoxyethoxy)ethoxy)ethoxy)-1,4-phenylene) tripyrrole (PyPhEG) was as described previously [39]. The ON probes were attached to the carboxylic acid groups on PyPhCOOH, as detailed below in section 2.3. PyPhEG was used as a co-monomer with PyPh-ON, on the presumption (not further investigated in this work) that the ethylene glycol units on PyPhEG would afford some antifouling properties to the sensing film[40].

2.2 Fabrication of screen-printed carbon electrodes (SPCE)

The sensor fabrication steps are presented in Scheme 1. The electrodes were designed to have a 2 mm diameter working electrode (WE), a reference electrode (RE) and a counter electrode (CE), as shown in the photograph in the Scheme 1(B). The carbon layer for all three electrodes was printed using BQ 242 carbon ink on a Mylar substrate, using a screen-printer (DEK1202) with manual control of the squeegee, as shown in Scheme 1(A i). The printed electrodes were cured in an oven at 130°C for 15 min. Ag/AgCl ink was brushed onto the end of the printed carbon RE (ca. 2 mm), then cured at 130°C for 20 min. Kapton tape, as an insulating layer, was applied to cover the electrode tracks, excluding the contact pads (Scheme 1 (A ii)). As shown in Scheme 1(C), scanning electron microscopy (SEM) revealed the rough morphology of the SPCE surface. The electrochemically estimated real surface area of the SPCEs (Supporting Information, Figure S2) was 0.043±0.003 cm^2, indicating a roughness factor of 1.4±0.1.

2.3 Attachment of ss-ON probes to PyPhCOOH monomer and electropolymerisation of the sensing CP layer onto SPCE

Covalent attachment of the single-stranded (ss-ON) probe to PyPhCOOH monomer is described in detail in[6]. In short, 100 µL of 200 µM PyPhCOOH monomer in THF solution was incubated with 100 µl of PBS (pH 6.5) containing EDC (20 mM) and NHS (10 mM) at 28°C for 1 h under N_2, followed by addition of 100 µL of 1 mM ss-ON probe for another 1 h [25]. After ON probe attachment, THF was evaporated under N_2 and the remaining aqueous solution, without further purification, was stored at -20 °C and used within 24 h. The final electropolymerisation solution contained 50 µM PyPhON, 500 µM PyPhEG, and 0.1 M sodium para-toluene sulfonate (NaToS) in 2 ml DMF/PBS (1:1), giving a PyPhEG:PhPyON ratio of 10:1. DMF was included to aid solubility of the co-monomer PyPhEG. For a 50:1 ratio, to afford a lower probe density, the concentration of PyPhEG monomer was kept at 500 µM, while the PyPhON concentration was adjusted accordingly. Before electropolymerisation, 20 µL of the monomer solution was pipetted onto the SPCE, fully covering the WE, RE and CE.

A potential of 0.8 V was applied to the WE for 30 s, unless otherwise stated, to electropolymerise the CP film onto the WE. The charge passed was 0.16±0.04 mC, giving an estimated thickness of poly(PyPhEG-*co*-PyPyON) of 20±5 nm, assuming uniform surface coverage. The estimation of thickness is provided in the SI. Scheme 2 gives a chemical structure model for the polymer. Oxidation of the polymer results in the formation of a radical cation[56]. A model for the charge-transfer reaction at the polymer-solution interface is a charge exchange with a radical cation trapped at the polymer-solution interface: Scheme 2B.

2.4 Detection of synthetic ss-ONs as target DNA

As shown in Scheme 1 (A iv), poly(PyPhEG-*co*-PyPhON)-based sensors were first incubated in HPB for 5 min prior to target ON detection. The EIS readout (see below) from this step was used as the baseline (R_{ct}^0) to normalize the EIS signal to the ON target solutions. Poly(PyPhEG-*co*-PyPhON) modified SPCE was incubated with 100 µL ON target solutions in HPB (in 1.5 mL Eppendorf vials) at 39.5 °C for 5 min (unless otherwise stated).

The electrodes were then washed with HPB and EIS measurements undertaken in a 20 µL drop of $K_3[Fe(CN)_6]/K_4[Fe(CN)_6]$ (10 mM each) redox couple in HPB deposited on the sensor surface. The impedance data were measured and collected over a frequency range from 1 Hz to 100 kHz, with 10 mV sinusoidal excitation amplitude at an applied bias potential of 0.14 V *vs.* Ag/AgCl (painted) as RE. The bias potential was determined from the CV measurements of poly(PyPhEG-*co*-PyPhON) modified SPCE as the potential of zero net current, as shown in Figure S1. In total, 85 and 81 independent sensors were tested for C-ON and Nc-ON, respectively. For titration measurements, working up from the lowest to the highest concentration, a single electrode was used, progressively repeating the sequence: removal of the drop of redox couple solution, washing of the electrode, incubation with the next oligonucleotide solution, then finally measurement in the redox couple solution.

2.5 Detection of specific DNA in bacterial lysates

The bacterial lysates were kindly supplied by Assoc. Prof. Simon Swift (The University of Auckland, Department of Molecular Medicine and Pathology). *E. coli* BL21 was used as the complementary 'target' and *Salmonella enterica* serovar Typhimurium (obtained from ATCC: https://www.atcc.org/products/all/14028.aspx#generalinformation) as the non-complementary control. A short probe sequence (Table 1) was designed by comparison of the known genomic sequences to be fully complementary to a 22-mer sequence found in *E. coli* BL21 with only partial complementarity to *Salmonella* (for at most 10 of the 22 nucleotides). The lysates were prepared by heating live bacterial solutions at 95 °C for 5 min and filtering through a 0.22 µm syringe filter before further dilution in HPB. After the EIS baseline was measured in a 20 µL HPB drop containing $K_3[Fe(CN)_6]/K_4[Fe(CN)_6]$ (10 mM each) redox couple, 50 µL of the bacterial lysate was heated at 95°C for 5 min to denature dsDNA[41]. This was then mixed immediately with room temperature deionised water in a 1.5 mL Eppendorf tube to dilute as required. Mixing decreased the solution temperature to approximately 60°C. Poly(PyPhEG-*co*-PyPhON)-modified SPCE was then immediately dipped into the solution and incubated at 39.5°C for 5 min. The electrodes were then washed with HPB and EIS measurements were carried out in a 20 µL drop of $K_3[Fe(CN)_6]/K_4[Fe(CN)_6]$ (10 mM each) redox couple in HPB deposited on the sensor surface.

2.6 Quartz crystal microbalance with dissipation (QCM-D) measurements

Gold (100 nm thick) coated quartz crystals (QSX301) were sonicated sequentially in ethanol and deionized water (Milli-Q, 18.2 MΩ.cm at 25°C) for 15 min each. A 5:1:1 vol ratio solution of deionized water, ammonia (25%) and hydrogen peroxide (30%) was heated to 75 °C and the sonicated quartz crystals were then added for 5 min. The crystals were then removed from the solution and rinsed thoroughly with deionised water before being dried with nitrogen gas [42]. A Poly(PyPhEG-*co*-PyPhON) film was then electropolymerized onto the surface of the cleaned gold-coated crystals after which they were transferred to the chamber of a Q-sense analyzer instrument (Biolin Scientific). Solutions of ON-targets or Non-ON targets in HPB were introduced into the chamber and allowed to bind with the ON probes on the poly(PyPhEG-*co*-PyPhON) film. The flow rate of all tested solutions was continuous at 65 µL/h for all the steps. The changes in quartz crystal frequency (Δf) and dissipation (D) were measured.

2.7 Computational method

The sensor was modelled as a 50^3 array of resistors drawn at random from a log-normal distribution. The conductance between opposite faces of the cube, applying cyclic boundary conditions for the other cube faces, was calculated using the relaxation method of Kirkpatrick[43], as described in detail by Williams and Pratt[44]. 400 different realisations of a random array with given mean and standard deviation were computed. Response was computed by altering the resistance change between each node relative to the unaltered resistance, with the magnitude of the relative change between each node also drawn at random from a lognormal distribution. Calculations were performed using VBA within an Excel spreadsheet. The VBA code is given in the SI.

3. Results and discussion

3.1 QCM-D confirmation of specific hybridization to the pre-functionalised electropolymerised film

The method for attachment of a capture probe to a sensor surface employed here is very different from that usually practiced, in which a sensor surface is first prepared and then a capture probe is conjugated. The functionalization of ON to the monomer of PyPhCOOH has been investigated and characterised by our group[6,8]. Here, the functionalization is done "off-chip", before polymerization, thus very significantly simplifying the route to mass manufacture. Therefore, confirmation (independently of electrochemical measurement) that the ON-functionalised electropolymerised film indeed specifically binds the target, was sought using QCM-D. The frequency precision of 0.01 Hz corresponds to a mass change of 0.025 ng/cm^2, in turn corresponding to 4.8x10^{-13} mol/cm^2 of ON (or, if all in solution, to 30 nM). This frequency precision dictated the concentration range to be explored which, though comparable to many literature reports, is significantly greater than the detection sensitivity of the electrochemical method reported below. Figure 1(A) shows the frequency change after flowing 10 µM and 50 µM C-ON or Nc-ON solutions over the poly(PyPhEG-*co*-PyPhON) modified crystal in the QCM-D flow cell. The introduction of C-ON solutions resulted in a decrease in the quartz crystal frequency, corresponding to an increase in the mass on the crystal surface (Figure 1(C)). To remove any non-specifically bound C-ON, HPB was subsequently introduced into the QCM-D chamber. The final mass change was 0.62 (0.25 Hz) and 2.11 (0.84 Hz) ng/cm^2 for 10 µM C-ON and 50 µM C-ON solutions after considering the hydration of ss-ON and ds-ON[45], corresponding to 1.7x10^{13} C-ON/cm^2 and 5.6 x10^{13} C-ON/cm^2, respectively. Figure 1 (C) gives a comparison of the mass change in response to C-ON and Nc-ON solutions passed through the flow cell. The resulting mass change was two- and six-times larger for 10 µM and 50 µM C-ON target solutions, respectively, compared to that for Nc-ON. These results confirm that the majority of the signal comes from specific DNA hybridization, while some residual non-specific adsorption of ONs occurs.

The changes in dissipation values (0.02x10^{-6} and 0.027x10^{-6}) after introducing 10 µM and 50 µM C-ON solutions, respectively (Figure 1(B)), mirror the quartz crystal frequency changes. The changes in dissipation after exposing the film to the solution of C-ON reflect the formation of a more rigid layer of dsDNA, upon hybridization of the C-ON to the surface-bound ON probe[46, 47]. Moreover, the ΔD/Δf after binding with 10 µM C-ON (0.08 x10^{-6} Hz^{-1}) was higher than that of 50 µM C-ON (0.03 x10^{-6} Hz^{-1}), indicating the increase of rigidity after more formation of a larger number of dsDNA on the surface [46].

3.2 Impedance response of the poly(PyPhEG-*co*-PyPhON) modified SPCE DNA sensor to synthetic single-stranded ON targets

The Nyquist diagram for the unmodified SPCE in the presence of the redox couple (Figure S3) showed a simple Randles equivalent circuit with a charge transfer resistance that was significantly variable from one electrode to another, in the range 5000-7000 Ω. Polymer modification changed the equivalent circuit to that generally used to describe the electrochemical impedance of a semiconductor-redox electrode involving charge transfer through surface states [48]. Figure 2 shows titration series on single electrodes, for both complementary and non-complementary ON, with impedance fitted to this equivalent circuit.

In this circuit model, the elements are assigned to the resistance along the electrode connector tracks, R_s, the resistance of the polymer film, R_{film}, the charge transfer resistance between the redox couple (diffusion impedance, W) and interface states, $R_{interface}$, a geometric capacitance due to the film, C_{film}, and a capacitance associated with the interface states, $C_{interface}$. Both R_{film} and $1/C_{film}$ varied linearly with increase of polymerization time (Figure S4) consistent with the expected linear increase of film thickness with polymerization time following an initial nucleation and spreading phase; $R_{interface}$ and $C_{interface}$ varied less markedly (Table S1) also as expected. The slight depression of the low-frequency semicircle in the Nyquist plots, due to the parallel combination of $R_{interface}$ and $C_{interface}$, is consistent with the effect of roughness of the conducting polymer surface, which may increase with increasing polymerization time. The effect of the complementary ON was marked, being observable in this particular series starting at 10 fM concentration. The effect of non-complementary ON was much smaller.

Figure 3 shows the variation of circuit element values with ON concentration, derived from the data of Figure 2. The resistances R_{film} and $R_{interface}$ varied logarithmically with concentration, giving both a high sensitivity and a wide dynamic range. The response extended to the concentration range probed above by QCM-D. The element ascribed to the resistance of the polymer film varied more strongly and indeed contributed the major part of the response. The film capacitance was constant and consistent with that expected for a thin organic layer. The capacitance $C_{interface}$ was, as expected, much higher: in the range 30 – 100 μF for different electrodes but not detectably dependent on ON concentration.

The value of R_{film} for different electrodes was significantly variable. Figure 4 shows that the distribution of values was log-normal, broadening and shifting with increasing concentration of complementary ON. The resistance change in response to the presence of complementary ON was approximately linearly related to the 'zero' resistance (in the absence of ON) though with significant scatter.

In view of the linear dependence of ΔR_{film} on $R_{film,0}$, the ratio $\Delta R_{film}/R_{film,0}$ was taken as the sensor response, and in view of the variability the question asked: what concentration could reliably be distinguished by a single-use sensor from the non-specific signal due to non-complementary ON? In Figure 5, results from a large number of single-use sensors are presented as violin and box-and-whisker plots. In Table 2, for the different datasets the probability that mean (t-test) and variance (F-test) are the same, assuming normal distributions, and probability that the distributions are the same using the non-parametric Kolmogorov-Smirnov (K-S) and Mann-Whitney (M-W) tests, is presented. Here, 'blank' refers to the case where the test solution contained no ON, and thus tests for signal change caused by drift of unknown origin resulting from the manipulation of the device. Figure 5 also shows the effect of varying PyPhEG:PyPhON (ratio of diluent to probe on the surface) (Figure 5(B)), the polymerization time (Figure 5(C)) and incubation time (Figure 5(D)).

Although there is a significant scatter in the results, the analysis confirms: (1) the results for 1 pM Nc-ON and blank are the same; (2) a significant signal over both the blank and 1 pM Nc-ON for complementary ON at concentration of 1 pM and a significant increase of signal with increasing concentration of complementary ON; (2) significant specificity for complementary over non-complementary ON at the same concentration; (3) although the variance of the different distributions is essentially the same, there is broadening of the signal distribution over

that for the blank, that increases with increasing concentration for the complementary ON and that is also observable for the non-complementary ON at 100 pM.

The probe density did not have a significant effect over the range investigated. The polymerisation time (translating into the thickness of the polymer) was marginally optimal at 30 s, where the distribution of signal values was also broadest; at the longest polymerization time explored, the mean signal was significantly diminished and the distribution of signal values significantly narrowed. The average thickness of the polymer film for 30 sec of polymerisation time was estimated to be 20±5 nm[49].

A short detection time is considered a key parameter in developing disposable and portable DNA sensors for field use, where the time from sampling to results is critical. The incubation time was investigated by incubating the sensor with 100 pM C-ON solution (Figure 5 (D)). The sensor response, $\triangle R_{film}/R_{film,0}$, after 5 min incubation time reached ca. 70% of the maximum signal (taken as after 60 min) and provided sufficient compromise between the signal intensity and time of analysis.

3.3 Sensor response to bacterial lysate

The sensor response to bacterial lysate fitted well to the equivalent circuit of Figure 2(C). Data and fitted curves are given in the Figure S5, Table S2 and S3. Figure 6 shows the variation in the fitted parameters for titration series on single electrodes, for the specific target *E. coli* BL21 and for the control *Salmonella*. There is a clear specific signal in the film resistance, R_{film}, with a detectable difference from the measurement in buffer at 5×10^3 CFU/mL. With increase of lysate concentration, the film capacitance also shows a decrease in response to the specific target. The response shown to *Salmonella* is much smaller. Figure 6(C) compares the distribution of response on multiple single-use electrodes expressed as $\Delta R_{film}/R_{film}^0$ at different concentrations of the bacteria. The statistical evaluation is given in Table 3.

The results show that single use electrodes could reliably distinguish 10^4 CFU/mL of *E. coli* from the buffer blank. Single use electrodes could also reliably distinguish $5x10^5$ CFU/mL of *E. coli* BL21 from 10^4 CFU/mL, and from *Salmonella* at the same concentration. *Salmonella* spp. at $5x10^5$ CFU/mL also gave a result that was statistically significantly greater than the blank, but not at 10^4 CFU/mL. Given the length of the bacterial genomes (*E. coli*: 4.6×10^6 nucleotides; *Salmonella*: ~4.9×10^6 nucleotides) some cross-sensitivity due to small mismatches with the probe sequence is not surprising. A concentration of 10^4 CFU/mL is ~10^{-17}M. Passage through the 0.22 μm filter would have sheared the DNA, into fragments of unknown length, possibly from as little as 5 kbases but more typically 50 to 100 kbase[50-52]. Thus, the concentration of DNA being detected in the *E. coli* BL21 bacterial lysate would be on the scale of 10^{-15} – 10^{-16} M. Overhangs of long fragments hybridised to the surface may themselves hybridise to other fragments, potentially leading to a surface DNA gel, which would account for the change in film capacitance at higher lysate concentration seen for the specific target, *E. coli*.

3.4 Response model for change in film conductivity

Our results show hybridisation detection primarily through variation in the resistance of the polymer film, with a smaller effect on the rate of the interfacial charge transfer. The effect on the interfacial reaction rate would be consistent with the simple Donnan exclusion mechanism[7]. The effect on the polymer film resistance gives a detectable signal at much lower concentration

and is consistent with modulation of charge trapping in the polymer at the polymer-solution interface[7, 29]. This is the same mechanism deduced by Wijeratne et al.[53] for the rate of a redox reaction at a CP-electrolyte interface[53]. The charge transport through the polymer layer is viewed as percolation through a network of junctions between nanoparticulate clusters. Microscopy of the polymer films indeed shows that they comprise a network of nanoparticles of size scale a few nm[29, 30]. The effect of hybridization of DNA to the surface would be to change the charge on the electrolyte side of the semiconductor-electrolyte junction. If the DNA charge is not screened by the electrolyte, then a compensating charge would be found on the semiconductor side. According to the classical theory for semiconductor-electrolyte junctions, this charge would be provided by fixed, ionized donor or acceptor states within the semiconductor with an accompanying change in charge carrier concentration[54]. The charge carrier concentration would be modulated near to the interface, and a change in rate of redox reactions would result from this change in charge carrier concentration[48]. This model, however, is not consistent with our results. The charge carriers in the CP are positive polarons, positively-charged radical cation species, localized on the polymer chain[55, 56]. These are also the species that mediate the redox reaction at the interface (Scheme 2B). A negative surface charge from bound DNA would increase the surface concentration of surface polarons so a decrease in charge transfer resistance at the interface would be expected. This is not observed. Certainly, control of the interfacial reaction rate as a consequence of an increase in uncompensated negative charge contributed by surface-bound DNA is consistent with the results, and explains the very large sensitivity to bacterial lysate, where the captured fragments would be long, giving a large uncompensated bound charge[25]. Therefore, a model relating surface charge to bulk conductivity, in which a negative surface charge causes a decrease in conductivity, is needed. One characteristic of CPs is that the dopant species are ions – negatively charged in this case – which would be mobile within the polymer structure, in contrast to the case of a crystalline semiconductor. Hence, a plausible model is that increase of negative surface charge leads to a dipolar charge distribution within the polymer beneath the surface: the surface-bound charge repels the negative donor species from the surface and traps polarons at the surface, decreasing the film conductivity immediately below the surface. The model is a modification of that given by Kannan et al.[29]. The effect will depend on the nanostructure of the CP film - the effect could be more marked at junctions between nanocrystals – and the effect might be very variable across the surface and variable in depth below the surface.

3.5 Interpretation through the study of random resistor networks

Figure 4 shows that the distribution of film resistance approximated log-normal. This distribution arises in the description of many natural phenomena because many natural growth processes are driven by the accumulation of many small percentage changes which become additive on a log scale[57]. In this case, the determining process is assumed to be the random assembly of polymer nanoparticles, as envisaged by Wijeratne et al. If the conductivity between individual particles was controlled by an activation barrier, with barrier height uniformly distributed, then the individual conductivities would be log-normally distributed. The resistance exhibited by individual realisations of the assembly of particles would therefore itself expected to be log-normally distributed. However, an effect of the distribution of individual resistances might be the occurrence of ‘critical paths’ of low resistance, analogous to a percolation threshold. A true percolation threshold as described by Wijeratne et al. was not observed in the present work[53]. Kirkpatrick[58] studied the properties of a cubic array of

resistors. When the resistance values are sampled at random from an appropriately chosen distribution, the effect of 'critical paths' may be observed. However, a percolation threshold as such may not be found as a consequence of the varying importance of current flow along 'non-critical paths' [8]. In order to understand further the properties of the CP film as a sensor, we have explored the distribution of resistance observed for a cubic network of resistors, where each resistor value is drawn at random from a log-normal distribution. Two features are of note from Figure 4: the distribution is broad; and there is a slight shift to higher resistance of the modal resistance of the experimental results from the modal resistance of the best-fitting log-normal. Results for the simulation using a cubic network of resistors are given in Figure 7. These showed: (1) that to obtain a broad distribution as observed experimentally, the underlying distribution of resistances of the network connections needed to be extremely broad (standard deviation of ln(resistance) ≈ 6); (2) that as the underlying resistance distribution broadened, the mode of the observed resistance distribution shifted to higher resistance than the mode of the fitted log-normal – there was a tail to the distribution at lower resistance.

These distributions show the effect of 'critical paths' through the cube: rare paths where the faces of the cube are connected predominantly through low-value resistors. The effect is signaled by the appearance in the distribution of a tail to low values of resistance. The tail becomes more marked as a consequence of the imposition of a 'response': the random formation of critical paths becomes more important as a consequence of the random increase in value of the resistors in the network relative to their unperturbed value. These effects can arguably be discerned in the experimental distributions.

3.6 Model for logarithmic dependence on solution oligonucleotide concentration

A logarithmic effect of solution oligonucleotide concentration was observed experimentally, giving rise to a very wide dynamic range. If a linear response model is assumed for the resistances in the network, then a power-law response for the network is obtained, as generally found for resistor network models[43, 58] and as shown by other types of conductimetric sensors [59]. Figure 7B shows this, and also shows that the response is modified for realisations where the resistance is low and hence dominated by critical paths. The logarithmic response to solution ON concentration is not therefore captured by the random resistor model with a uniform response of all resistors in the network. A logarithmic response requires a logarithmic dependence of the resistance of individual elements of the network. The model developed above requires then a logarithmic dependence on solution concentration of ON of the uncompensated surface charge resulting from ON binding. A potential explanation comes from consideration of the adsorption isotherm describing the ON binding. A simple model is a Temkin-type isotherm, where the adsorption free energy depends on surface coverage, in this case through variation of the surface charge causing a variation of the surface potential with respect to the bulk solution:

$$\theta/(1-\theta) \approx c\, exp\left(-\left(\Delta G_{ads}^{0} + \left((zen_{max}\theta)^2/C_{interface}\right)\right)\right) \qquad (1)$$

Here, θ denotes the fractional coverage of surface binding sites by ON, and the bound surface charge is thus $q\theta$, where q is the charge per bound molecule; c denotes the solution concentration of ON, ΔG_{ads}^{0} the adsorption Gibbs energy at zero coverage. The additional charge bound to the surface, $q = zen_{max}\theta$ where e is the electronic charge, z the charge per bound molecule and n_{max} the number of bound molecules per unit area at full coverage ($\theta = 1$).

The term $\left((zen_{max}\theta)^2/C_{interface}\right) = \left(q^2\theta/C_{interface}\right)$ accounts for the effect on the binding energy as the surface charge increases, increasing the surface potential. It increases rapidly as the surface coverage increases. At very low coverage, equation 1 gives a linear dependence of coverage (hence bound charge) on concentration. However, the effect of the surface potential change soon begins to dominate, especially if z is large, as is the case with bound oligonucleotides or DNA fragments, giving rise to a logarithmic dependence of bound charge on solution concentration, making the model developed above consistent with the experimental observations.

3.7 Significance of the results

The significance of the results is that a highly sensitive and specific DNA detection, previously demonstrated to be compatible with PCR amplification and offering detection of low copy numbers with few amplification cycles[30], is achieved with a device which is mass-manufacturable at low cost. The concept design shown in figure 8 is based on the results given here and those reported in ref 30. The main issue for the sensors is the distribution of sensitivity for different electrodes. The modelling indicates that this may be an inherent characteristic of these sensors, dependent on the control of nanostructure in the electropolymerized film, and dependent on the uniformity or otherwise of response across the connections between CP nanoparticles that are assumed to control the film resistance.

Variation across the surface in the electropolymerisation reaction rate could lead to areas that are either imperfectly decorated with CP, or not decorated at all, or sites where the modifying probe ON has been in part buried within a thicker layer of the polymer. Polymer nanostructure, coverage and thickness, and local probe density would affect the local value of $R_{film,0}$ and local exposed probe density would affect the signal, $\triangle R_{\text{film}}/R_{\text{film,0}}$. Variability of the electropolymerisation may be connected to variability of transport and reaction across the electrode surface, particularly porosity, cracks and any variations in the type of carbon exposed. A further possible artifact is non-specific adsorption of oligonucleotides causing a time-dependent wetting in cracks and porosity. Screen-printing inks from different manufacturers vary in the detailed composition of the carbon and the binders, and the surface composition; specifically, the ratio of carbon to binder exposed at the surface, as well as the porosity, varies with the details of the printer setup as well as with details of methodology in mixing and drying. Improvements in manufacture can be anticipated, however, given that the possibility of mass-manufacture has now been demonstrated. Other studies have reported methods such as oxygen plasma treatment or laser surface glazing as routes to improve repeatability[60, 61]. Given that screen-printed carbon might produce intrinsically unreliable electrodes[62], other carbon-based electrode fabrication technologies, such as laser-scribing of graphene on flexible substrates [63,64] may provide superior alternatives, or electrodes such as gold-coated mylar could be considered.

Conclusion

We have demonstrated the fabrication at significant scale of a portable, single-use DNA-sensing strip with very high detection sensitivity based on poly(PyPhEG-*co*-PyPhON)-modified screen-printed electrodes. The poly(PyPhEG-*co*-PyPhON) was electropolymerised from the ON probe pre-attached monomer. We have shown that the signal is generated as a result of the surface charge-dependence of the polymer film resistance and have described a model for the response based on percolation in a random resistor array.

Statistically significant detection at 1 pM ss-ON concentration has been demonstrated for 82 single-use sensor strips (and selectivity with another >80 sensor strips), independently measured. Statistically significant detection of DNA in bacterial lysate has been demonstrated at 10^4 CFU/mL (concentration on fM – aM scale) for single-use sensor strips. In titration experiments on particular strips, the detection limit was lower. In general, SPCEs with poly(PyPhEG-*co*-PyPhON) modification as a basis for these biosensors show potential for detection of DNA with simple, portable instrumentation and single-use sensor strips. Precise control of nanostructure and capture-probe exposure in the electropolymerized films is a key challenge to overcome. The method is suitable for low-cost industrial-scale fabrication, and the detection sensitivity and selectivity could be further extended by the use of these devices in conjunction with the previously-described electrochemical PCR method[30].

Acknowledgement:

We would like thank Dr Nitish Dhirubhai Patel from The University of Auckland, Dept of Electrical and Computer Engineering for his assistance with equipment. This work was funded by Auckland UniServices Ltd and the MacDiarmid Institute for Advanced Materials and Nanotechnology, New Zealand.

Reference:

1. H. Peng, L. Zhang, C. Soeller and J. Travas-Sejdic, *Biomaterials*, **30**, 2132 (2009).
2. M. H. Naveen, N. G. Gurudatt and Y.-B. Shim, *Appl. Mater. Today*, **9**, 419 (2017).
3. A. Ramanavičius, A. Ramanavičienė and A. Malinauskas, *Electrochim. Acta*, **51**, 6025 (2006).
4. N. Aydemir, J. Malmström and J. Travas-Sejdic, *Phys. Chem. Chem. Phys.*, **18**, 8264 (2016).
5. J. Travas-Sejdic, N. Aydemir, B. Kannan, D. E. Williams and J. Malmström, *J Mater Chem B .*, **2**, 4593 (2014).
6. N. Aydemir, E. Chan, P. Baek, D. Barker, D. E. Williams and J. Travas-Sejdic, *Biosens. Bioelectron.*, **97**, 128 (2017).
7. B. Kannan, D. E. Williams, M. A. Booth and J. Travas-Sejdic, *Anal. Chem.*, **83**, 3415 (2011).
8. T. E. Kerr-Phillips, N. Aydemir, E. W. C. Chan, D. Barker, J. Malmström, C. Plesse and J. Travas-Sejdic, *Biosens. Bioelectron.*, **100**, 549 (2018).
9. H. Peng, C. Soeller, N. Vigar, P. A. Kilmartin, M. B. Cannell, G. A. Bowmaker, R. P. Cooney and J. Travas-Sejdic, *Biosens. Bioelectron.*, **20**, 1821 (2005).
10. H. Korri-Youssoufi, F. Garnier, P. Srivastava, P. Godillot and A. Yassar, *J. Am. Chem. Soc.*, **119**, 7388 (1997).
11. L. A. Thompson, J. Kowalik, M. Josowicz and J. Janata, *J. Am. Chem. Soc.*, **125**, 324 (2003).
12. E. de Boer and R. R. Beumer, *Int. J. Food Microbiol.*, **50**, 119 (1999).
13. F. Darain, S.-U. Park and Y.-B. Shim, *Biosens. Bioelectron.*, **18**, 773 (2003).
14. M. A. Bangar, D. J. Shirale, W. Chen, N. V. Myung and A. Mulchandani, *Anal. Chem.*, **81**, 2168 (2009).
15. B. Zhu, O. A. Alsager, S. Kumar, J. M. Hodgkiss and J. Travas-Sejdic, *Biosens. Bioelectron.*, **70**, 398 (2015).
16. S. J. Park, J. Lee, S. E. Seo, K. H. Kim, C. S. Park, S. H. Lee, H. S. Ban, B. D. Lee, H. S. Song, J. Kim, C.-S. Lee, J. Bae and O. S. Kwon, *Sci. Rep.*, **10**, 3772 (2020).
17. A. Sargent and O. A. Sadik, *Electrochim. Acta*, **44**, 4667 (1999).
18. E. Sheikhzadeh, M. Chamsaz, A. P. F. Turner, E. W. H. Jager and V. Beni, *Biosens. Bioelectron.*, **80**, 194 (2016).
19. M. Gębala and W. Schuhmann, *ChemPhysChem*, **11**, 2887 (2010).
20. Y. Yang, C. Li, L. Yin, M. Liu, Z. Wang, Y. Shu and G. Li, *, Anal. Chem.*, **6**, 7579 (2014).
21. K. Hu, D. Lan, X. Li and S. Zhang, *Anal. Chem.*, **80**, 9124 (2008).
22. N. Hong, L. Cheng, B. Wei, C. Chen, L. L. He, D. kong, J. Ceng, H.-F. Cui and H. Fan, *Biosens. Bioelectron.*, **91**, 110 (2017).
23. V. Vogiazi, A. de la Cruz, W. R. Heineman, R. J. White and D. D. Dionysiou, *Anal. Chem.*, **93**, 812 (2021).
24. S. Tajik, H. Beitollahi, F. G. Nejad, I. S. Shoaie, M. A. Khalilzadeh, M. S. Asl, Q. Van Le, K. Zhang, H. W. Jang and M. Shokouhimehr, *RSC Adv.*, **10**, 37834 (2020).
25. M. A. Booth, S. Harbison and J. Travas-Sejdic, *Biosens. Bioelectron.*, **28**, 362 (2011).
26. B. Zhu and J. Travas-Sejdic, *Analyst*, **143**, 687 (2018).
27. T. H. M. Kjällman, H. Peng, C. Soeller and J. Travas-Sejdic, *Anal. Chem.*, **80**, 9460 (2008).
28. K. Lacina, J. Sopoušek, V. Čunderlová, A. Hlaváček, T. Václavek and V. Lacinová, *Electrochem. commun.*, **93**, 183 (2018).

29. B. Kannan, D. E. Williams, C. Laslau and J. Travas-Sejdic, *Biosens. Bioelectron.*, **35**, 258 (2012).
30. N. Aydemir, H. McArdle, S. Patel, W. Whitford, C. W. Evans, J. Travas-Sejdic and D. E. Williams, *Anal. Chem.*, **87**, 5189 (2015).
31. F. Farabullini, F. Lucarelli, I. Palchetti, G. Marrazza and M. Mascini, *Biosens. Bioelectron.*, **22**, 1544 (2007).
32. J. C. Liao, M. Mastali, Y. Li, V. Gau, M. A. Suchard, J. Babbitt, J. Gornbein, E. M. Landaw, E. R. B. McCabe, B. M. Churchill and D. A. Haake, *J Mol Diagn*, **9**, 158 (2007).
33. A. L. Suherman, B. Rasche, B. Godlewska, P. Nicholas, S. Herlihy, N. Caiger, P. J. Cowen and R. G. Compton, *ACS Sens.*, **4**, 2497 (2019).
34. P. Pasakon, J. P. Mensing, D. Phokaratkul, C. Karuwan, T. Lomas, A. Wisitsoraat and A. Tuantranont, *J. Appl. Electrochem.*, **49**, 217 (2019).
35. B. Huang, L. Ji, B. Liang, Q. Cao, T. Tu and X. Ye, *Analyst*, **144**, 3282 (2019).
36. K. C. Honeychurch and J. P. Hart, *Trends Analyt Chem*, **22**, 456 (2003).
37. G. Cui, S. J. Kim, S. H. Choi, H. Nam, G. S. Cha and K.-J. Paeng, *Anal. Chem.*, **72**, 1925 (2000).
38. M. I. González-Sánchez, B. Gómez-Monedero, J. Agrisuelas, J. Iniesta and E. Valero, *J. Electroanal. Chem.*, **839**, 75 (2019).
39. E. W. C. Chan, P. Baek, S. M. Tan, S. J. Davidson, D. Barker and J. Travas-Sejdic, *Macromol. Rapid Commun.*, **40**, 1800749 (2019).
40. X. Fan, L. Lin and P. B. Messersmith, *Biomacromolecules*, **7**, 2443 (2006).
41. B. Zhu, M. A. Booth, P. Shepherd, A. Sheppard and J. Travas-Sejdic, *Biosens. Bioelectron.*, **64**, 74 (2015).
42. R. Khadka, N. Aydemir, C. Carraher, C. Hamiaux, D. Colbert, J. Cheema, J. Malmström, A. Kralicek and J. Travas-Sejdic, *Biosens. Bioelectron.,* **126**, 207 (2019).
43. S. Kirkpatrick, *Reviews of Modern Physics*, **45**, 574 (1973).
44. D. E. Williams and K. F. E. Pratt, *Sens. Actuators B Chem.*, **70**, 214 (2000).
45. M. Bastos, V. Castro, G. Mrevlishvili and J. Teixeira, *Biophys. J.*, **86**, 3822 (2004).
46. W. Tang, D. Wang, Y. Xu, N. Li and F. Liu, *ChemComm*, **48**, 6678 (2012).
47. D. Meléndrez, T. Jowitt, M. Iliut, A. F. Verre, S. Goodwin and A. Vijayaraghavan, *Nanoscale*, **10**, 2555 (2018).
48. Z. Hens, *J. Phys. Chem*, **103**, 122 (1999).
49. N. Lassalle, P. Mailley, E. Vieil, T. Livache, A. Roget, J.P. Correia, and L.M. Abrantes, *J. Electroanal. Chem*, **509**, 48 (2001).
50. T. Klingström, E. Bongcam-Rudloff and O. V. Pettersson, *bioRxiv*, 254276 (2018).
51. A. Joneja and X. Huang, *Biotechniques*, **46**, 553 (2009).
52. M. A. Quail, in *Encyclopedia of Life Sciences (ELS)*, John Wiley & Sons, Ltd. (2005).
53. K. Wijeratne, U. Ail, R. Brooke, M. Vagin, X. Liu, M. Fahlman and X. Crispin, *PNAS*, **115**, 11899 (2018).
54. J. N. Zemel, *Sens. Actuators*, **1**, 31 (1981).
55. J. L. Brédas, J. C. Scott, K. Yakushi and G. B. Street, *Phys. Rev. B Condens. Matter*, **30**, 1023 (1984).
56. J. L. Bredas and G. B. Street, *Acc. Chem. Res.*, **18**, 309 (1985).
57. https://en.m.wikipedia.org/wiki/Log-normal_distribution#. 2.
58. S. Kirkpatrick, *Phys. Rev. Lett.*, **27**, 1722 (1971).
59. G. Chabanis, I. P. Parkin and D. E. Williams, *Meas Sci Technol*, **14**, 76 (2002).
60. S. C. Wang, K. S. Chang and C. J. Yuan, *Electrochim. Acta*, **54**, 4937 (2009).
61. M. D. Osbome, B. J. Seddon, R. A. W. Dryfe, G. Lagger, U. Loyall, H. Schäfer and H. H. Girault, *J. Electroanal. Chem*. **417**, 5 (1996).

62. P. Fanjul-Bolado, D. Hernández-Santos, P. J. Lamas-Ardisana, A. Martín-Pernía and A. Costa-García, *Electrochim. Acta*, **53**, 3635 (2008).
63. G. Xu, Z. A. Jarjes, H.-W. Wang, A. R. J. Phillips, P. A. Kilmartin and J. Travas-Sejdic, *ACS Appl. Mater. Interfaces*, **10**, 42136 (2018).
64. G. Xu, Z. A. Jarjes, V. Desprez, P. A. Kilmartin and J. Travas-Sejdic, *Biosens. Bioelectron.*, **107**, 184 (2018).

Figures and tables:

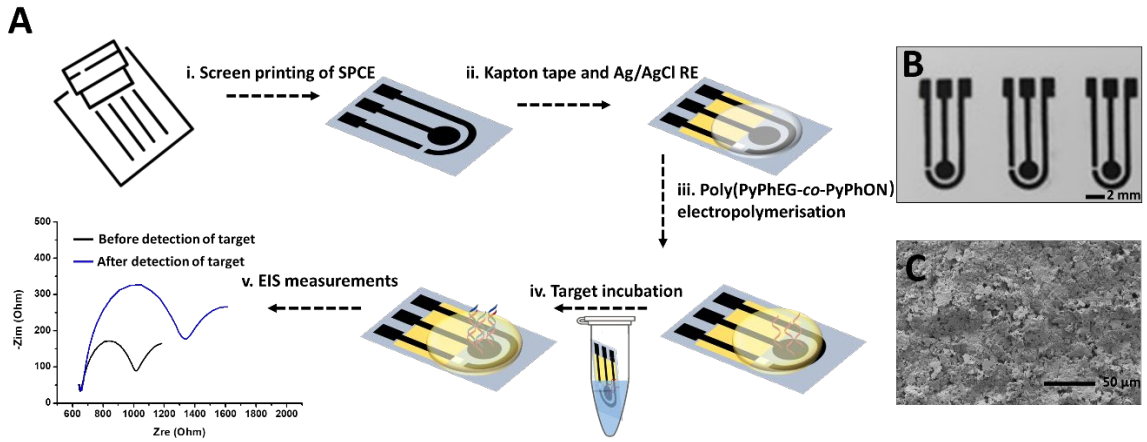

Scheme 1. (A) Scheme outlining the sensor fabrication process and target DNA detection: (i) screen printing of SPCEs; (ii) covering the electrode tracks by Kapton tape and 'painting' of Ag/AgCl paste that serves as a reference electrode; (iii) electropolymerisation of poly(PyPhEG-*co*-PyPhON) onto the SPCE in a 20 µL droplet of co-monomer solution deposited on the electrode ; (iv) incubation of the CP-modified SPCE in 100 µL of the target solution in a 1.5 mL Eppendorf tube, and (v) measuring EIS before and after incubation of the electrode in the target solution; EIS was performed in a 20 µL drop of 10 mM $K_3[Fe(CN)_6]/K_4[Fe(CN)_6]$. (B) Optical photograph of SPCEs; and (C) SEM image of a bare SPCE surface, showing the rough morphology of SPCE.

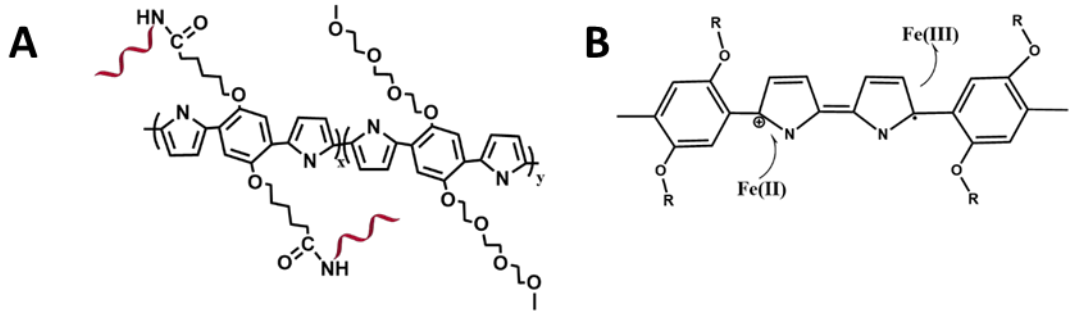

Scheme 2. (A) Chemical structure model for the functionalized CP; (B) Model for the charge transfer reaction between solution redox couple and oxidized polymer.

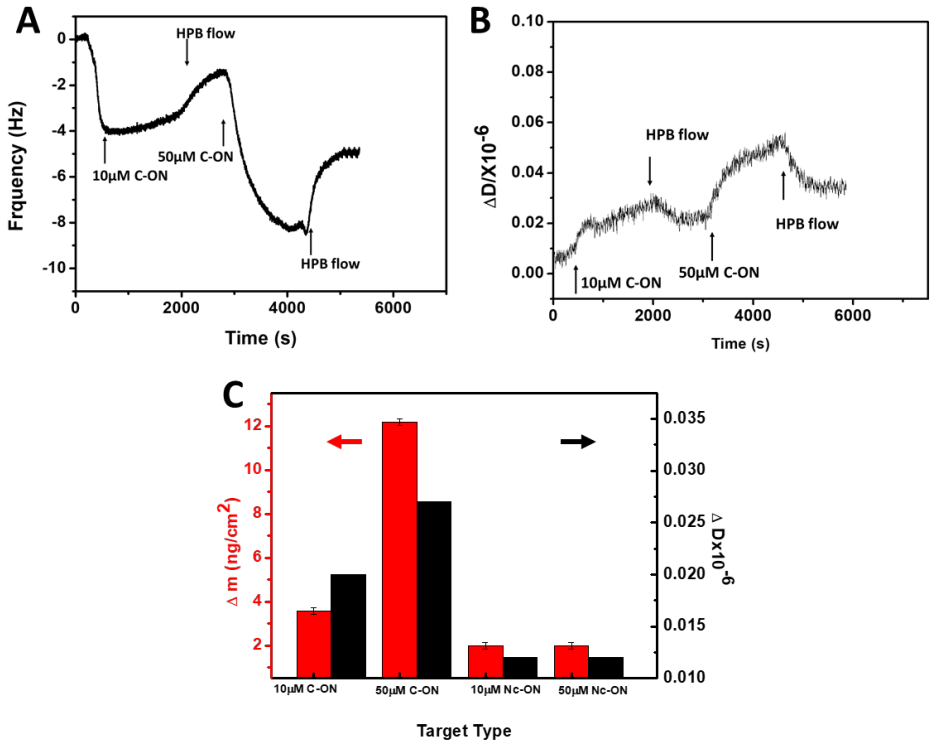

Figure 1. (A) The change in QCM frequency of poly(PyPhEG-*co*-PyPhON) (10:1)-modified gold-coated QCM quartz surface upon introducing 10 μM and 50 μM C-ON target into the detection chamber. (B) Dissipation shifts (the data were smoothed using the Savitzky-Golay method). (C) Comparison in mass change (red) and dissipation shift (black) from complementary (C-ON) and non-complementary (Nc-ON) solutions (n=3).

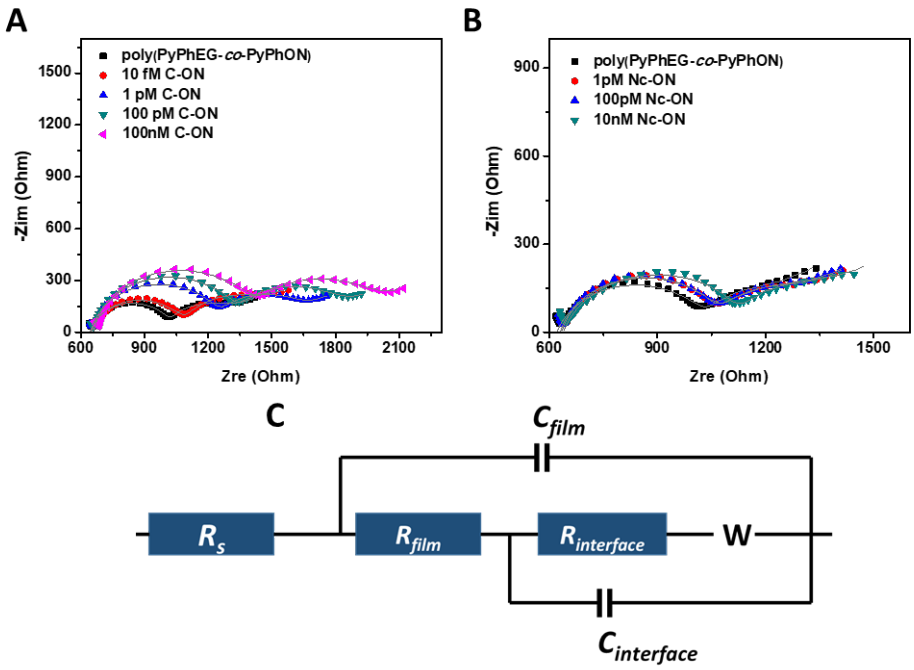

Figure 2. Impedance response to increasing concentration of oligonucleotide. A): complementary; B): non-complementary. C): equivalent circuit. Lines are the fit, points are the experimental data. Fitting was done with constant phase elements, which showed that both could be represented as simple capacitors for the purpose of interpretation (power, a, = 0.95 – 1 for C_{film} and 0.85 – 0.92 for $C_{interface}$. The geometric capacitance of the electrode assembly, in parallel with the entire circuit and giving rise to the additional feature at the highest frequency, is not fitted.

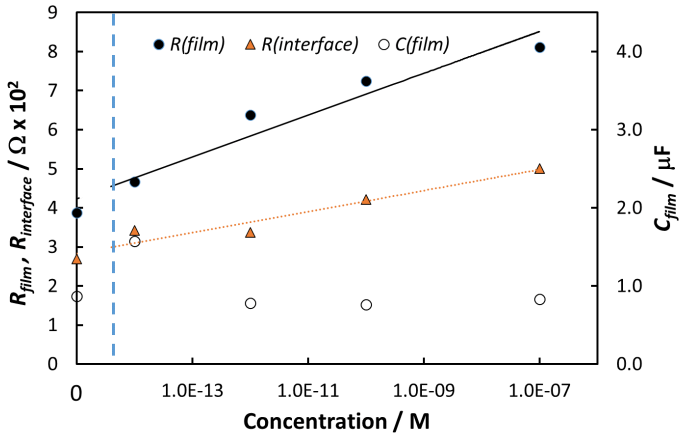

Figure 3. Variation of equivalent circuit element values with the concentration of complementary ON, for a single electrode measured in a titration series. R_{film} (closed circles), $R_{interface}$ (closed triangles) and C_{film} (open circles) determined by fitting to the equivalent circuit shown in Figure 2C, against solution oligomer concentration.

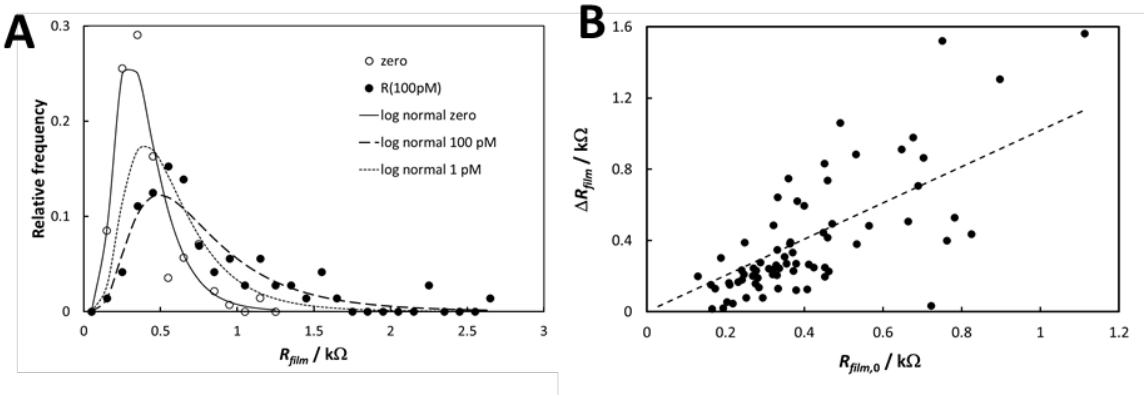

Figure 4. Distribution of film resistance measured for a large number of electrodes, and the change with increasing concentration of ON. A): Film resistance distribution fitted to log-normal (data points and fit shown for zero and 100 pM; fit only shown, for clarity, for 1 pM); B) Film resistance change caused by addition of 100 pM complementary ON: ΔR_{film} against film resistance in the absence of complementary ON ($R_{film,0}$). Each point is the result for a different electrode.

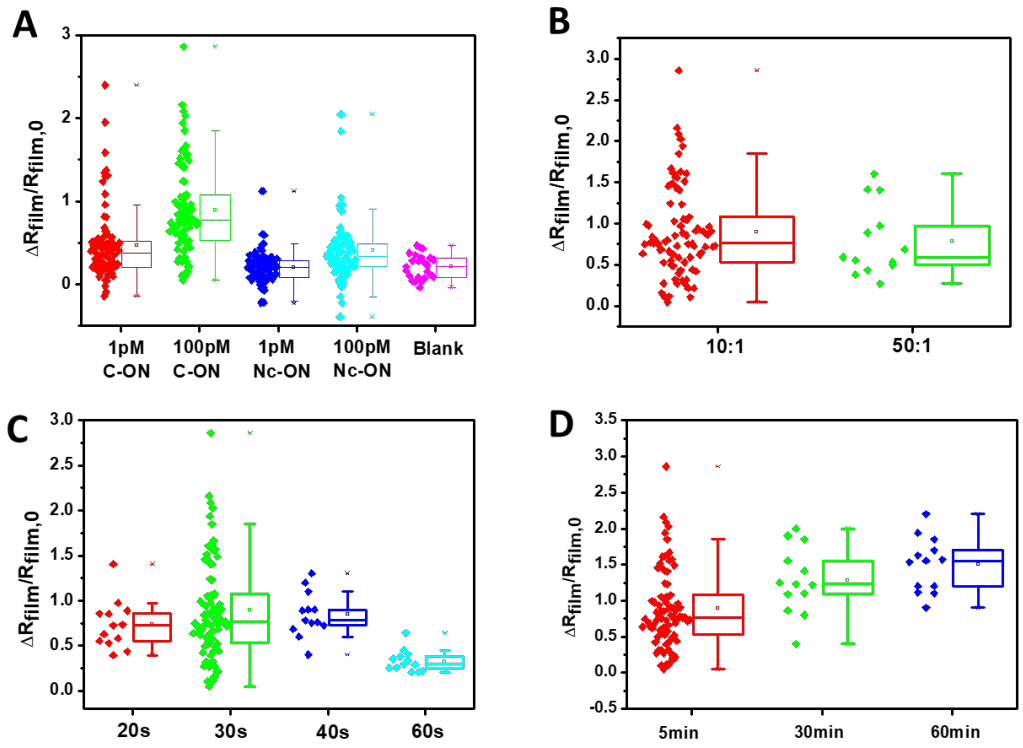

Figure 5. (A) Normalised responses of the poly(PyPhEG-*co*-PyPhON) (10:1) modified SPCE sensors, $\triangle R_{film}/R_{film,0}$; box-and-whiskers plots show the data points, mean, median and upper and lower quartiles for each condition, where each measurement is on a fresh electrode (n=85 for C-ON, 81 for Nc-ON and 24 for blank). Incubation time was 5 min and probe density 10:1 PyPhEG:PyPhON in the polymerisation solution. (B) Effect of the probe density on the poly(PyPhEG-*co*-PyPhON) sensor signal, $\Delta R_{film}/R_{film,0}$, after incubation with 100 pM C-ON, with molar ratios of PyPhEG:PyPhON in the polymerization solution 10:1 or 50:1 (n = 85 for 10:1, and n=12 for 50:1). (C) Changes in sensor signal $\triangle R_{film}/R_{film,0}$ as a function of polymerization time after incubation with 100 pM C-ON (n = 85 for 30s, and n=12 for 20s, 40s and 60s). (D) $\triangle R_{ct}/R_{ct}^{0}$ of poly(PyPhEG-*co*-PyPhON) (10:1) after incubation with 100 pM C-ON *vs*. detection time.

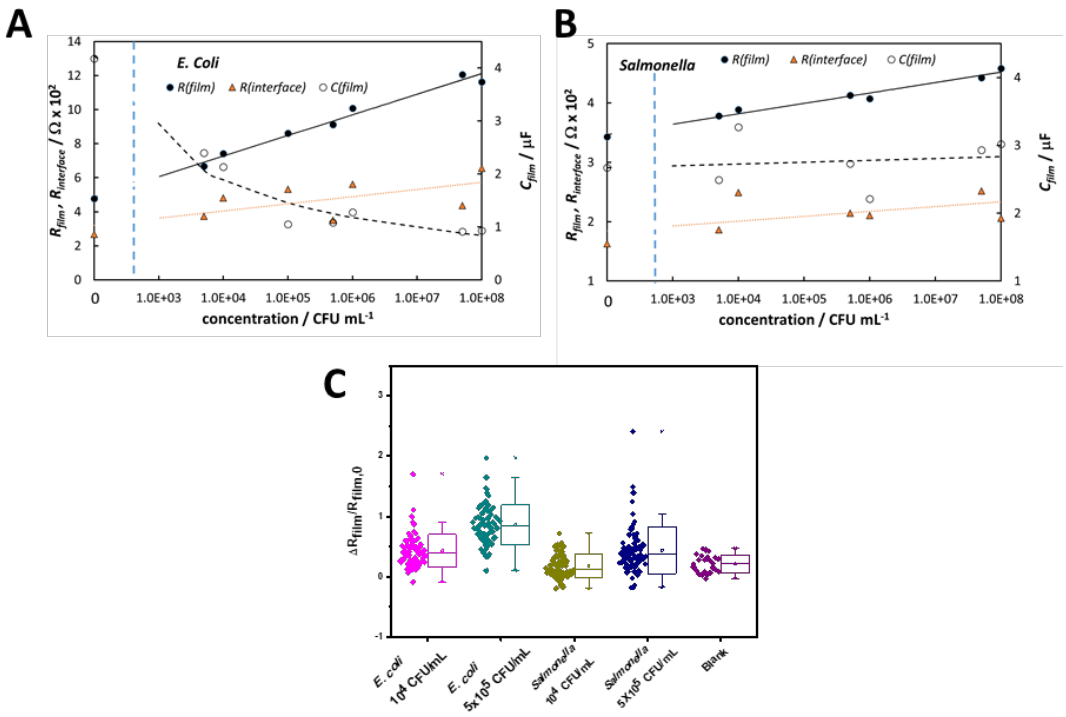

Figure 6. Fitted parameter values for the equivalent circuit of Figure 2C of poly(PyPhEG-*co*-PyPhON) (10:1) modified SPCE determined in a titration series of concentration of (A) *E. coli* and (B) *Salmonella* Lysate (solid line); (C) $\triangle R_{\text{film}}/R_{\text{film},0}$; box-and-whiskers plots show the data points, mean, median and upper and lower quartiles for each condition of the poly(PyPhEG-*co*-PyPhON) (10:1) modified SPCE sensors after detection of 10^4 and $5x10^5$ CFU/ml *E. coli* and *Salmonella* lysate, and for measurement on a buffer blank. Each measurement is on a fresh electrode.

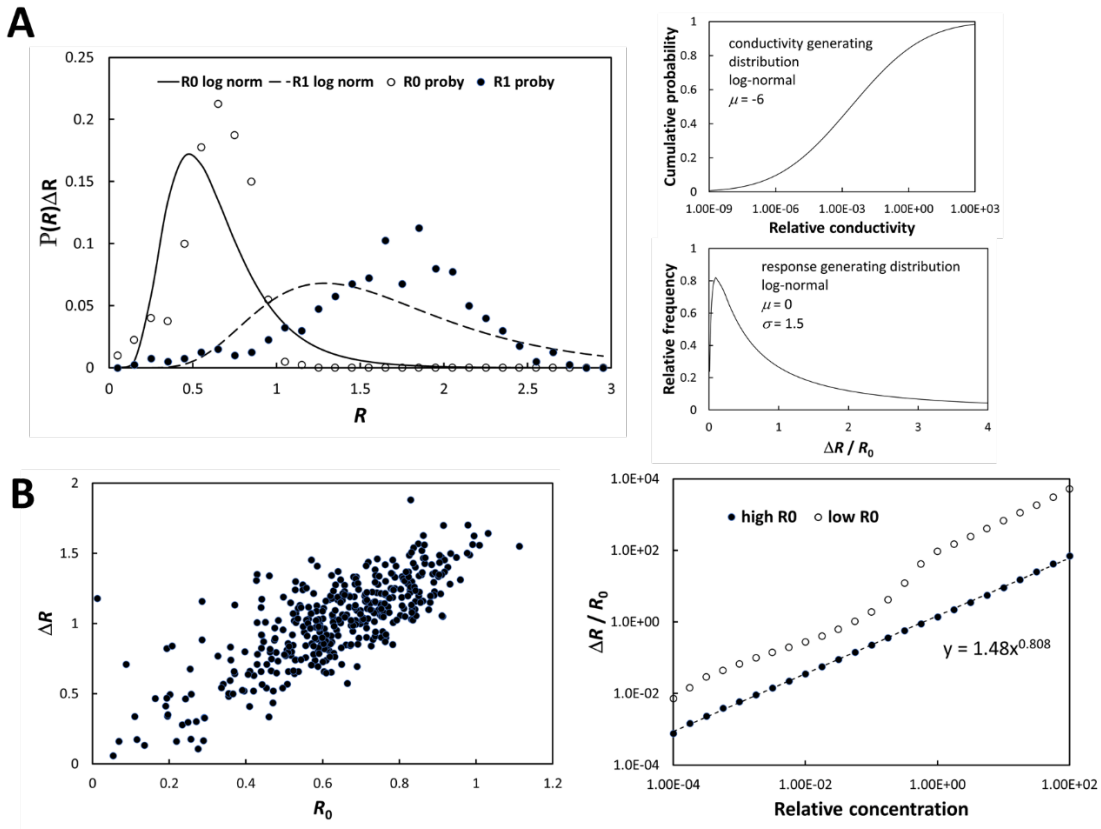

Figure 7. Model response for 50^3 cubic array of resistors where the resistance (conductance) of each individual resistor is drawn at random from a log-normal distribution, and the relative resistance change representing the response is also drawn at random from a log-normal distribution, evaluated for 400 different realisations. (A) Resistance distributions for the 'zero', R_0, and 'response', R_1 . Inset: conductance distribution and relative response distribution of individual elements of the array; (B) Resistance change ΔR and relative resistance change $\Delta R/R_0$ caused by the imposed response according to the response distribution in (A), (left), against the 'zero' resistance, R_0, for each of the 400 realisations, for relative concentration $C = 1$, and (right) against relative concentration according to the assumed linear response law for each resistor in the network $\Delta R/R_0 = sC$ where s denotes the sensitivity drawn from the distribution in (A) – the two curves are for cubes with R_0 at the lower and upper values found in the set.

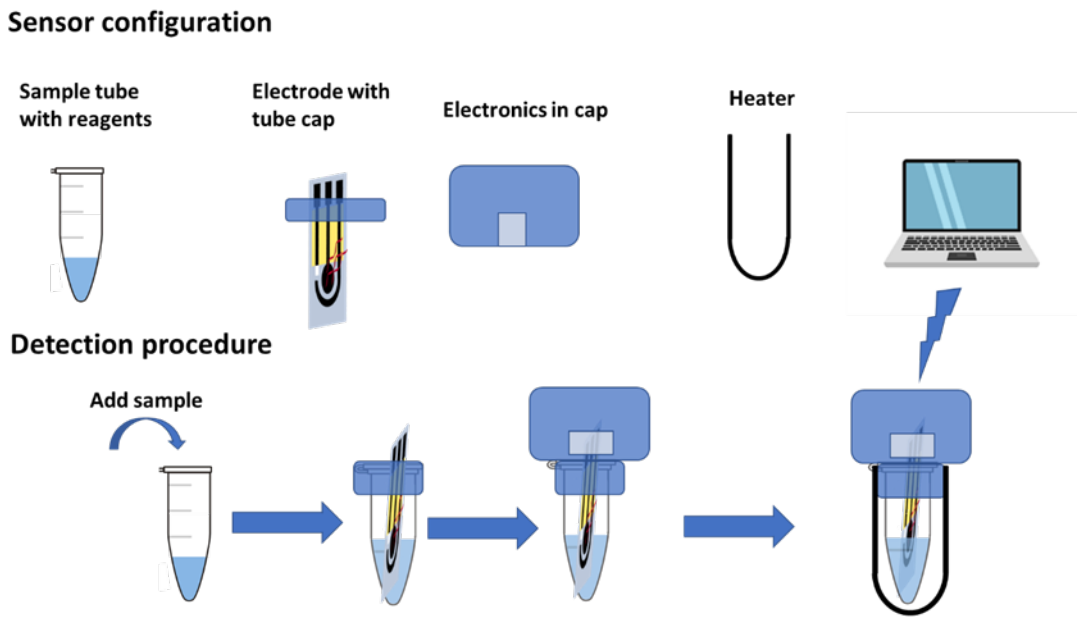

Figure 8. Design concept for rapid, point-of-use measurement using e-PCR. The reagents required (ferri-ferrocyanide, DNA polymerase, primers, nucleotides and buffer salts) are supplied lyophilised in a sample tube to which aqueous sample is added. The electrode (as in Scheme 1) has the polymer precursor incorporated into a water-soluble gel and printed onto it, and is supplied moulded into a cap which fits tightly into the sample tube. The electronics necessary to control the electrochemistry clip onto the top of the assembly. The only operations required of the user are to add the sample into the tube, push in the electrode-carrying cap, then the cap containing the electronics and insert the assembly into the heater. Bluetooth connection to the control device activates the sequence shown in Scheme 1: first the electropolymerisation then the heating cycle and impedance measurement as described in ref 30.

Table 1. Sequences of synthetic oligonucleotide probes and targets used.

Oligonucleotide	**Modification**	**DNA sequences (5'-3')**
Single-stranded (ss)-ON probe	5' amino	GGAAGGATCGACAGATTTGATC
Complementary ON target (C-ON)	None	GATCAAATCTGTCGATCCTTCC
Non-complementary ON target (Nc-ON)	None	AGCTCGCGCGATATCGATCGAA
Probe specific to *E. coli* BL 21	5' amino	GGAAGGATCGACAGATTTGATC

Table 2. Statistical data for the sensing signals detecting synthetic ONs. For the datasets compared, probability that mean (t-test) and variance (F-test) are the same, assuming normal distributions, and probability that the distributions are the same using the non-parametric Kolmogorov-Smirnov (K-S) and Mann-Whitney (M-W) tests.

	1 pM C-ON	**100 pM C-ON**	**1 pM Nc-ON**	**1 pM C-ON and 100 pM C-ON**	**1 pM C-ON and 1 pM Nc-ON**	**100 pM C-ON and 100 pM Nc-ON**

	and Blank	and Blank	and Blank			
t- test	0.005	< 0.001	0.9	< 0.001	< 0.001	< 0.001
F-test	>0.99	>0.99	0.9	0.97	>0.99	0.99
K-S test	0.005	< 0.001	0.9	< 0.001	< 0.001	< 0.001
M-W test	<0.001	< 0.001	0.6	< 0.001	< 0.001	< 0.001

Table 3. Statistical comparisons of bacterial lysates. For the datasets compared, the probability that mean (t-test) and variance (F-test) are the same, assuming normal distributions, and the probability that the distributions are the same using the non-parametric Kolmogorov-Smirnov (K-S) and Mann-Whitney (M-W) tests are shown.

	10^4 CFU/mL *E. coli* BL21 and Blank	**$5x10^5$ CFU/mL *E. coli* BL21 and Blank**	**10^4 CFU/mL *Salmonella* and Blank**	**$5x10^5$ CFU/mL *Salmonella* and Blank**	**10^4 CFU/mL *E. coli* BL21 and $5x10^5$ CFU/mL *E. coli* BL21**	**10^4 CFU/mL *E. coli* BL21 and 10^4 CFU/mL *Salmonella***
t-test	< 0.001	< 0.001	0.4	0.06	< 0.001	< 0.001
F-test	0.001	< 0.001	0.2	< 0.001	0.09	0.003
K-S test	0.004	< 0.001	0.6	0.009	< 0.001	< 0.001
M-W test	< 0.001	< 0.001	0.3	0.001	< 0.001	< 0.001

TOC:

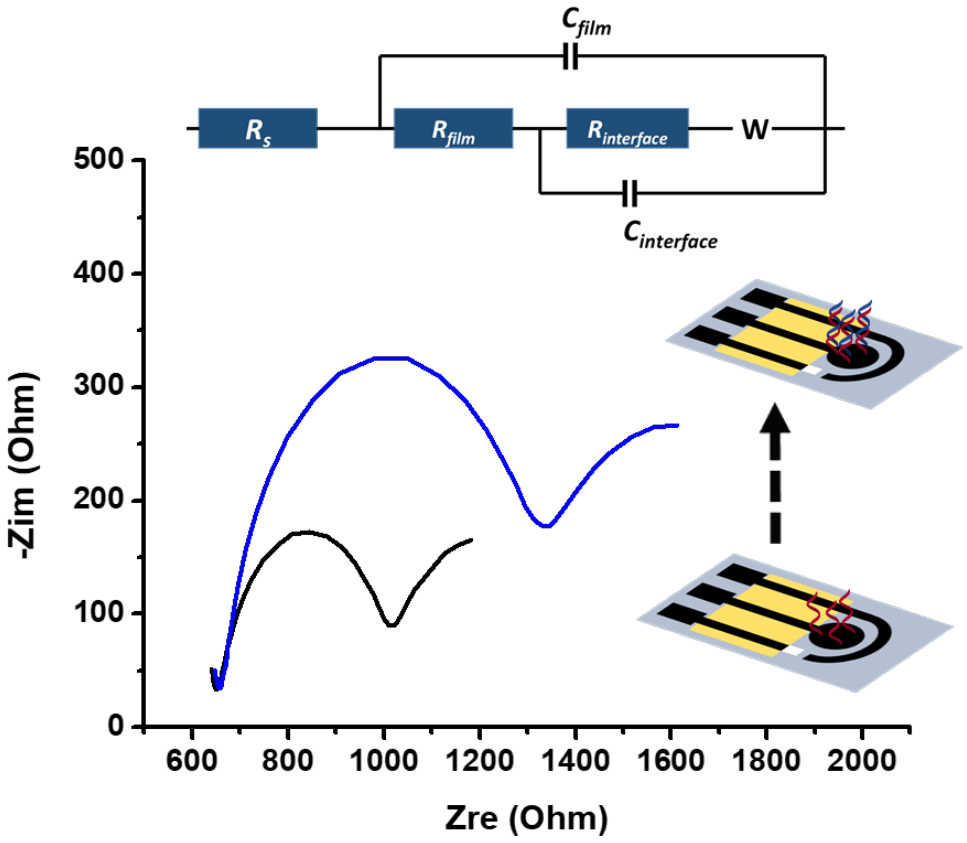
C_{film}
R_s
R_{film}
$R_{interface}$
W
$C_{interface}$
500
400
300
200
100
0
-Zim (Ohm)
600
800
1000
1200
1400
1600
1800
2000
Zre (Ohm)